www.czasopisma.pan.pl PAN www.journals.pan.pl
Chemical and Process Engineering 2015, 36 (1), 3-19
DOI: 10.1515/cpe-2015-0001

A MECHANISTIC MODEL OF A PASSIVE AUTOCATALYTIC HYDROGEN RECOMBINER

Antoni Rożeń*

Warsaw University of Technology, Faculty of Chemical and Process Engineering, Waryńskiego 1, 00-645 Warszawa, Poland

A passive autocatalytic hydrogen recombiner (PAR) is a self-starting device, without operator action or external power input, installed in nuclear power plants to remove hydrogen from the containment building of a nuclear reactor. A new mechanistic model of PAR has been presented and validated by experimental data and results of Computational Fluid Dynamics (CFD) simulations. The model allows to quickly and accurately predict gas temperature and composition, catalyst temperature and hydrogen recombination rate. It is assumed in the model that an exothermic recombination reaction of hydrogen and oxygen proceeds at the catalyst surface only, while processes of heat and mass transport occur by assisted natural and forced convection in non-isothermal and laminar gas flow conditions in vertical channels between catalyst plates. The model accounts for heat radiation from a hot catalyst surface and has no adjustable parameters. It can be combined with an equation of chimney draft and become a useful engineering tool for selection and optimisation of catalytic recombiner geometry.

Keywords: hydrogen, catalysis, laminar flow, natural convection, forced convection

1. INTRODUCTION

During normal operation of a light-water nuclear reactor (LWR), hydrogen is produced by water radiolysis. However, in the case of a severe accident (SA) in a nuclear power plant (NPP) such as overheating of a reactor core, a large amount of hydrogen can be released due to exothermal oxidation of zirconium fuel cladding. In any case, hydrogen accumulates in the water cooling system of the reactor and in the containment building (NEA/CSNI, 2014). Its distribution in the containment can be complex depending on the intensity of internal gas circulation. Consequently, local concentration of this combustible gas can exceed the flammability limit and result in accidental ignition followed by flame propagation in the reactor containment. Several methods are applied in NPP to mitigate the risk of hydrogen deflagration or even detonation, e.g.: controlled ignition, catalytic recombination conducted in PARs, injection of a neutral gas, forced gas circulation, removal of oxygen (IAEA-TECDOCs, 2001 and 2011). Among these methods, PARs have become a very important factor in emergency procedures for hydrogen removal in a growing number of NPPs since Fukushima-Daiichi nuclear accident in March, 2011.

A typical PAR is a metal box consisting of a system of vertical metal plates coated with a catalyst (e.g. platinum or palladium) in its lower part and an empty chimney section – Fig. 1. Instead of plates, a metal grid, a honeycomb structure or a granular bed can be used as the support for a thin micrometer catalyst layer. PARs are available in different sizes depending on dimensions and the number of catalytic plates or cartridges and the length of the chimney section (Areva, 2014).

*Corresponding author, e-mail: a.rozen@ichip.pw.edu.pl

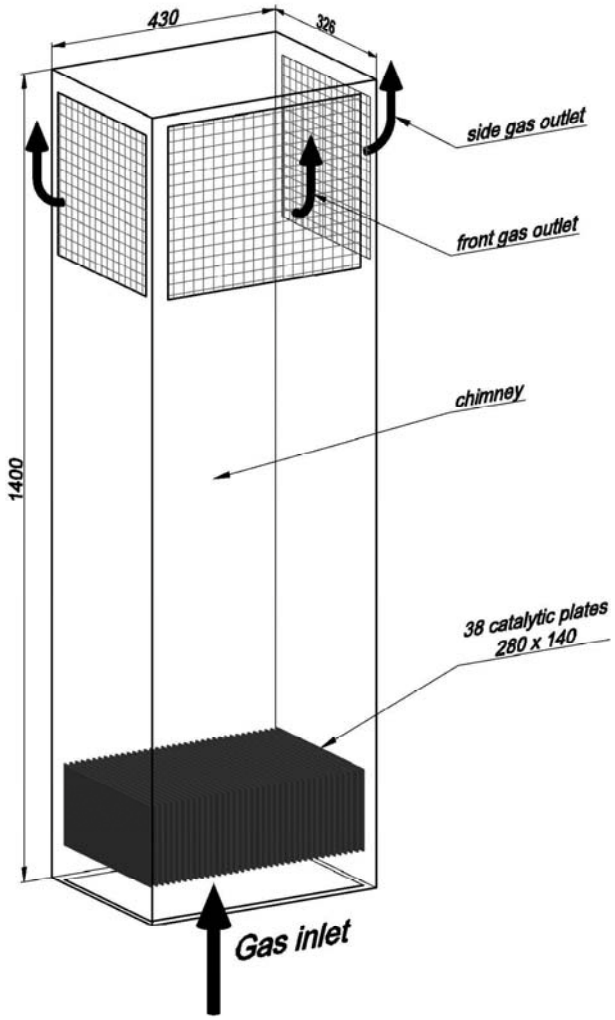

Fig. 1. Sketch of Areva FR1-380T recombiner; dimensions are given in millimetres

On the other hand, the PAR presented in Fig. 2 is a typical test recombiner with just four catalyst plates. Commercial recombiners produced e.g. by AECL, Areva or NIS can contain more than one hundred catalyst plates. The total number and placement of PAR units within containment structures should allow to obtain the desired coverage of the containment volume and the desired overall capacity. For example, in a large dry pressurised water reactor such as German PWR type KONVOI containment, 65 AREVA recombiners are installed (NEA/CSNI, 2014). Hydrogen and oxygen are adsorbed at catalyst active spots, recombine and create steam and heat (2.4×10^5 kJ/kmol of H_2). Reaction heat is released into the gas phase due to natural and forced convection. Hot, humid gas flows into the upper empty section of PAR, where the chimney draft force accelerates gas convection. PAR requires neither external power input nor constant control, which is especially important in the case of SA (Reinecke et al., 2010). Recombiners begin to work as soon as local hydrogen concentration exceeds approximately 1% v/v and continue their operation as long as sufficient hydrogen and oxygen are available. Catalyst ignition occurs spontaneously at normal or elevated pressure and at room or higher temperature. During operation, PARs produce vigorous natural mixing of gas in their vicinity.

The mathematical modelling of PAR behaviour by means of CFD methods has been conducted by many researchers, e.g. Gera et al. (2012), Heitsch (2000), Prabhudharwadkar et al. (2011b), Reinecke et al. (2010) and recently by Meynet et al. (2014). Now it has reached a satisfactory level mostly in the case of stationary PAR operation. On the contrary, few mechanistic models of PAR have been formulated so far allowing for quick engineering calculations. For example, Avakian and Braillard (1999) and Jimenez et al. (2007) modelled PAR as a continuously stirred tank reactor assuming that the

gas phase inside PAR is perfectly mixed. However, the key catalytic reactions have non-linear kinetics according to Fridell et al. (1994) and Rinemo et al. (1997). Additionally, according to results of CFD simulations (Reinecke et al., 2010; Rożeń, 2013), the fastest drop of hydrogen concentration takes place in a short entrance section of the channels between the catalyst plates where gas temperature and composition differ significantly from their average values inside the PAR box. Hence, the assumption that reactants are perfectly mixed in the gas phase may lead to miscalculations. Reinecke et al. (2005) formulated a more realistic model of PAR as a continuous plug flow reactor, where the recombination reaction is completely diffusion controlled. Material and heat balance equations were solved in this model in a two-dimensional space of a single channel. Relevant coefficients of heat and mass transfer were obtained by fitting numerical results to experimental data.

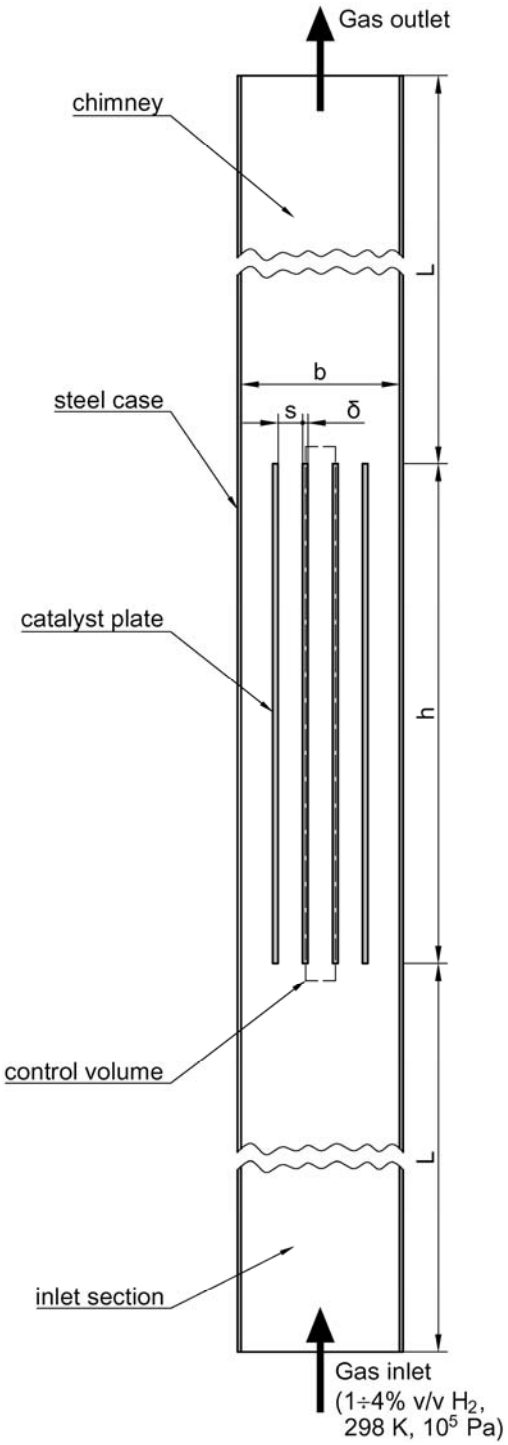

Fig. 2. Geometry of the test PAR unit used by Reinecke et al. (2005) and Drinovac (2006); b=0.046 m, h=0.143 m, l_1=l_2=0.18 m, s=0.0085 m, δ=0.0015 m

The main aim of this work is to present and validate a one-dimensional model of PAR. Following Reinecke et al. (2005) and Drinovac (2006), it is proposed to model the recombiner as a continuous plug flow chemical reactor. However, instead of calibrating the model with some experimental results, general correlations are used to calculate coefficients of heat convection from walls of vertical slits (Rohsenow et al., 1998). Coefficients of mass convection are obtained with a classical method of Taunton et al. (1970). In order to avoid assuming a priori that the entire PAR operates in the diffusion controlled regime, the kinetics of heterogeneous hydrogen recombination is directly implemented into the model. An expression for chimney draft force in the recombiner box is formulated and combined with the model. Then sample optimisation of the PAR geometry is performed. Model predictions are also compared with experimental results and results of CFD simulations obtained for the test recombiner.

2. MODEL DESCRIPTION

Passive autocatalytic recombiners are open flow systems which operate at ambient or elevated pressure characteristic for the reactor containment building; during accidents typical for LWRs like loss of coolant as a consequence of a rapture of steam piping, containment pressure can increase several times. Gas temperature inside PAR can vary from room temperature in the inlet section up to 400÷800 K in the chimney section depending on the inlet hydrogen concentration. In these conditions, components of the gas phase (nitrogen, oxygen, hydrogen and steam) are far from their critical point. Hence it could be assumed, following Reinecke et al. (2010) and Meynet et al. (2014), that density of the gas phase can be calculated from the ideal gas law. Other gas properties such as: thermal conductivity, dynamic viscosity and coefficients of molecular diffusivity were calculated in the present work from the kinetic theory of gas, while the specific heat of gas components was obtained from data available in the book of Poling et al. (2001). The specific heat of the gas mixture was calculated as the mass average.

PAR housing and plates, which are covered with washcoat platinum, are made from stainless steel in commercial and in laboratory recombiners. Density, specific heat and thermal conductivity of stainless steel depend on its grade. In this work, values of these properties typical for ferritic steel were adopted: ρ_s=7700 kg/m^3, $c_{p,s}$=460 J/(kg·K) and λ_s=25 W/(m·K) (Euro Inox, 2014).

Conditions for momentum, heat and mass transport in all vertical channels between the catalyst plates are virtually the same except for the side channels where gas has lower temperature and hydrogen concentration is higher. Results of CFD simulations performed for geometry similar to that shown in Fig. 2, indicate that the gas flow inside the channels between the catalyst plates is predominantly laminar even when the average gas velocity in the inlet section equals 1.6 m/s (Rożeń, 2013). This is so because turbulence of the gas stream entering narrow channels is quickly attenuated in the channel entrance region. Consequently, in the present model correlations of heat and mass transfer coefficients appropriate for laminar flow were adopted. It was also assumed that the central recombiner section can be modelled as a system of "n" identical vertical channels.

The longitudinal dispersion of enthalpy and gas components, heat exchange with the PAR surrounding, except heat radiation via the channels openings, and heat production by viscous forces were neglected in the present model version. Gas temperature and species concentration were assumed to be constant in the lateral channel cross-sections except thermal and concentration boundary layers developing at the channel walls. Temperature of the steel plates could vary in the vertical direction only and it was assumed to be equal to the catalyst temperature. All calculations were conducted for a stationary case and hydrogen recombining with oxygen at the catalyst surface only.

Hydrogen recombination at the catalyst surface proceeds according to an overall scheme

$$H_2 + \frac{1}{2}O_2 \rightarrow H_2O \tag{1}$$

and consists of at least 16 elementary reactions, which can be divided into three groups: adsorption, surface and desorption reactions (Fridell et al., 1994; Rinnemo et al., 1997). For low hydrogen concentration (less than 5% v/v) and low gas humidity, the full, complex kinetic model can be reduced to a single equation for hydrogen recombination rate (Prabhudharwadkar et al., 2011a)

$$\tilde{r}_{H_2} = 0.07311\sqrt{\frac{RT_w}{M_{H_2}}}\frac{c_{H_2}^2}{c_{O_2}} \tag{2}$$

This model is also known as simplified Kasemo's model and should not be used in case of oxygen deficiency. Another one-equation kinetic model known as Schefer's model assumes first order kinetics for the recombination reaction (Schefer, 1982)

$$\tilde{r}_{H_2} = 14\exp\left(\frac{-14.9\cdot 10^3}{RT_w}\right)c_{H_2} \tag{3}$$

This model gives lower values of the recombination rate than Kasemo's model. Comparison of calculation results obtained using Kasemo's and Schefer's model will be used in this study to find out if and how recombination kinetics affects the operation of PAR.

Enthalpy of hydrogen recombination reads

$$\Delta\tilde{H} = \sum_j \nu_j \tilde{H}_j \tag{4}$$

and in standard conditions (298 K, 10^5 Pa) it is equal to -2.42×10^5 kJ/kmol.

The main equations of the one-dimensional PAR model are as follows:

- the mass balance of i-th gas component

$$\dot{m}\frac{dw_i}{dx} = -\frac{k_i A_w (w_i - w_{w,i})}{h} \tag{5}$$

- the enthalpy balance of the gas phase

$$\dot{m}\frac{dH}{dx} = \frac{A_w}{h}\left[\alpha(T_w - T) + \Delta\tilde{H}\cdot\tilde{r}_{H_2}\right] \tag{6}$$

- the heat conduction equation for the catalyst plates

$$\lambda_s\frac{d^2T_w}{dx^2} = \frac{2}{\delta}\left[\alpha(T_w - T) + \Delta\tilde{H}\cdot\tilde{r}_{H_2} + q_r\right] \tag{7}$$

A control volume for heat and mass transport processes fully encloses a single channel in PAR as marked in Fig. 2 by a dashed line.

Enthalpy of a unit mass of an ideal gas mixture in Eq. (6) equals

$$H = \sum_j w_j H_j \tag{8}$$

Unknown a priori values of mass fraction of reactants in gas adjacent to the catalyst surface, $w_{w,i}$, can be calculated in two ways. It can be either assumed that the local recombination rate is totally controlled by mass convection towards the catalyst surface (Drinovac, 2006; Reinecke et al., 2005) or these unknowns can be determined from the following equations:

$$M_{H_2}\tilde{r}_{H_2} = k_{H_2}(w_{H_2} - w_{w,H_2}) \tag{9}$$

$$\frac{1}{2}M_{O_2}\tilde{r}_{H_2} = k_{O_2}(w_{O_2} - w_{w,O_2}) \tag{10}$$

$$M_{H_2O}\tilde{r}_{H_2} = -k_{H_2O}(w_{H_2O} - w_{w,H_2O}) \tag{11}$$

The heat of the exothermic reaction proceeding at the catalyst surface is: absorbed by the adjacent gas, irradiated to other solid surfaces, or conducted by the catalyst plates and other constituents of PAR.

Transport of heat from the hot catalyst surface to gas occurs due to natural convection caused by temperature difference and also due to forced convection induced by the chimney draft force. In order to account for both convection types, Churchill's rule was adopted to calculate the local heat transfer coefficient (Churchill, 1977)

$$\alpha = \left[(\alpha_n)^3 + (\alpha_f)^3\right]^{1/3} \tag{12}$$

The mean heat transfer coefficient of natural convection for the vertical slits equals

$$\bar{\alpha}_n = Nu_n \frac{\lambda}{s} \tag{13}$$

The Nusselt number for free convection depends on the Rayleigh and Prandtl numbers (Rohsenow et al., 1998, Chap. 4):

$$Nu_n = \left[\left(Ra/24\right)^m + \left(1.2C_l Ra^{0.25}\right)^m\right]^{1/m} \qquad m = -1.9 \tag{14}$$

$$Pr = \frac{\nu\rho c_p}{\lambda} \tag{15}$$

$$Ra = \frac{g\rho c_p \beta_T (\bar{T}_w - T_0)s^3}{\nu\lambda} \cdot \frac{s}{x} \tag{16}$$

$$C_l = 0.671\left[1 + \left(0.492/Pr\right)^{9/16}\right]^{-4/9} \tag{17}$$

Gas properties used in Eqs (13-17) should be calculated at the arithmetic mean of the inlet gas temperature and the mean wall temperature

$$T_m = \frac{T_1 + \bar{T}_w}{2} \tag{18}$$

The local heat transfer coefficient of natural convection in Eq. (12) was determined as

$$\alpha_n = \frac{1}{T_w - T}\frac{d}{dx}\left[\bar{\alpha}_n(\bar{T}_w - T_0)x\right] \tag{19}$$

Forced convection of heat from the catalyst surface to gas flow takes place in conditions of developing hydrodynamic and thermal boundary layers along the entire channel length. The local heat transfer coefficient for forced convection in such a case equals

$$\alpha_f = Nu_f \frac{\lambda}{2s} \tag{20}$$

and the Nusselt number depends on dimensionless channel length, the Prandtl and Peclet numbers (Rohsenow et al., 1998, Chap. 5):

$$Nu_{f,x} = 7.55 + \frac{0.024(x^*)^{-1.14}(0.0179Pr^{0.17}(x^*)^{-0.64} - 0.14)}{1 + 0.0358Pr^{0.17}(x^*)^{-0.64}} \tag{21}$$

$$x^* = \frac{x}{2sPe} \tag{22}$$

$$Pe = \frac{\dot{m}}{A} \cdot \frac{2sc_p}{\lambda} \tag{23}$$

Gas properties used in Eqs (20-23) should be calculated at the mean film temperature

$$T_f = \frac{\overline{T} + \overline{T}_w}{2} \tag{24}$$

Heat is also irradiated from the catalyst surfaces via the channel openings. The local radiative heat flux was found from the Stefan-Boltzmann law and the radiative heat balance

$$q_r = (1-\varepsilon_c)(1-F_{dx-s})\overline{q}_r + \varepsilon_c \sigma F_{dx-s}\left(\overline{T}_w^4 - T_e^4\right) \tag{25}$$

where the average radiative heat flux reads

$$\overline{q}_r = \frac{\sigma}{\frac{1}{\varepsilon_c} + \frac{1}{2F_{h-s}} - 1}\left(\overline{T}_w^4 - T_e^4\right) \tag{26}$$

The mean temperature of the catalyst plates was used to simplify derivation of Eqs (25-26). For the same reason, the emissivity of the surroundings was set to 1. The configuration factors of the surfaces emitting and absorbing heat radiation were found in engineering handbooks e.g. Rohsenow et al. (1998, Chap. 7):

- a horizontal strip of differential width dx on the catalyst plate and both channel openings

$$F_{dx-s} = 1 - \frac{1}{2}\left[\frac{x}{\sqrt{s^2 + x^2}} + \frac{h-x}{\sqrt{s^2 + (h-x)^2}}\right] \tag{27}$$

- the catalyst plate and both channel openings

$$F_{h-s} = \frac{1}{2}\left[1 + \frac{s}{h} - \sqrt{\left(\frac{s}{h}\right)^2 + 1}\right] \tag{28}$$

Transport of hydrogen and oxygen from the gas phase to the catalyst surface and steam in the opposite direction occurs in conditions of assisted natural and forced convection.

The mean mass transfer coefficient of natural convection for the walls of vertical slits equals

$$\overline{k}_{n,i} = Sh_{n,i}\frac{D_i\rho}{s} \tag{29}$$

Buoyant force is generated in the channel between the catalyst plates by the temperature difference and not by the concentration difference

$$\beta_T(T_w - T) >> \left|\beta_i(w_{w,i} - w_i)\right| \tag{30}$$

In these circumstances, the Sherwood number characterising the natural mass convection can be found, according to Taunton et al. (1970), directly from Eqs (14-17) by replacing the Nusselt with the

Sherwood number and multiplying the Rayleigh and Prandtl numbers with a modulus $(Sc_i/Pr)^{4/3}$. The Schmidt number in this dimensionless group has a definition

$$Sc_i = \frac{\nu}{D_i} \tag{31}$$

Forced convection of mass between the catalyst surface and the gas phase takes place in conditions of developing hydrodynamic and concentration boundary layers. The local mass transfer coefficient for forced convection in such a case equals

$$k_{f,i} = Sh_{f,i} \frac{D_i \rho}{2s} \tag{32}$$

The local Sherwood number for forced mass convection can be found, according to Bird et al. (2002, Chap. 22), from Eqs (21-23) by replacing: the Nusselt with the Sherwood number, the Prandtl with the Schmidt number and the thermal Peclet number with its concentration analog

$$Pe_i = \frac{\dot{m}}{A} \cdot \frac{2s}{\rho D_i} \tag{33}$$

As for assisted natural and forced heat convection, the local mass transfer coefficient of combined mass convection was estimated from the following equation

$$k_i = \left[(k_{n,i})^3 + (k_{f,i})^3 \right]^{1/3} \tag{34}$$

where the local coefficient of natural convection equals

$$k_{n,i} = \frac{1}{w_i - w_{w,i}} \frac{d}{dx} \left[\overline{k}_{n,i} (w_{0,i} - \overline{w}_{w,i}) x \right] \tag{35}$$

The governing differential balance equations of the PAR model (5-7) were integrated with the following boundary conditions for species concentration, gas temperature and heat flux:

- the channel entrance

$$x = 0 \quad w_i = w_{i,1} \quad T = T_1 \quad \lambda_s \frac{dT_w}{dx} = q_1 \tag{36}$$

- the channel exit

$$x = h \quad \lambda_s \frac{dT_w}{dx} = -q_2 \tag{37}$$

Heat fluxes at the lower and upper edges of the catalyst plate were set to:

$$q_1 = \alpha_1 \left[T_w(0) - T_1 \right] + \varepsilon_s \sigma \left[T_w(0)^4 - T_e^4 \right] \tag{38}$$

$$q_2 = \alpha_2 \left[T_w(h) - T_2 \right] + \varepsilon_s \sigma \left[T_w(h)^4 - T_e^4 \right] \tag{39}$$

The heat transfer coefficients α_1 and α_2 at the plate ends were calculated from correlations available in Rohsenow et al. (1998, Chap. 4).

The differential Eqs (5-7) with the boundary conditions (36-37) were integrated numerically by means of a simple forward Euler method with variable step control. The local recombination rate was determined by solving Eqs (9-11) by means of the Levenberg-Marquardt method (Press et al., 1992).

Gas flowing through the PAR box must obey a macroscopic momentum balance. Hence, if there is no gas accumulation (stationary flow), the total force exerted by steel walls on gas reads

$$F = A_1 (p_1 + \rho_1 v_1^2) - A_2 (p_2 + \rho_2 v_2^2) - m_g g \tag{40}$$

The static gas pressures at the inlet and outlet of the recombiner are equal to:

$$p_1 = p_0 - \frac{1}{2}\rho_1 v_1^2 - \frac{1}{2}\zeta_1 \rho_1 v_1^2 \tag{41}$$

$$p_2 = p_0 - \rho_1 g(l_1 + h + l_2) - \frac{1-\zeta_2}{2}\rho_2 v_2^2 \tag{42}$$

If the cross-sections of the inlet and outlet ducts are the same ($A_1=A_2=A_d$), like in the case of the test recombiner (Fig. 2), then eliminating pressures p_1 and p_2 from Eqs (40-42) gives the chimney draft equation

$$F = \rho_1 g(l_1 + h + l_2)A_d - m_g g + \left(1 - \frac{1+\zeta_1}{2}\right)A_d \rho_1 v_1^2 - \left(1 - \frac{1-\zeta_2}{2}\right)A_d \rho_2 v_2^2 \tag{43}$$

The minor loss coefficients in Eq. (43) for the box entrance and exit depend on the recombiner geometry. In the case of the test device shown in Fig. 2, the following values were used: ζ_1=0.5 and ζ_2=1 (Crane, 2009).

Wall force F can be extracted from pressure and velocity fields in a CFD post processing phase; otherwise, it has to be estimated as a superposition of several factors responsible for pressure losses in PAR. The main contribution to the wall force acting on gas gives the viscous drag in the channels between the catalyst plates but the viscous drag in the inlet and outlet ducts should also be taken into account. Accuracy of the wall force estimation can be additionally improved by corrections for the channel entrance and exit obtained from local momentum balance of the gas phase.

$$F \cong A_d \Delta p_1 + (nA)\Delta p + A_d \Delta p_2 + \left(F_{c,1} + F_{c,2}\right) \tag{44}$$

The pressure loss in subsequent PAR regions should be calculated as for hydrodynamically developing flow using e.g. a method formulated by Shah (1978). According to this method, the pressure loss in the channel formed by the parallel plates equals:

$$\Delta p = 4f \frac{h}{d_h}\frac{\bar{\rho} v^2}{2} \tag{45}$$

where

$$f = \frac{3.44}{Re\sqrt{x^+}} + \frac{24 + 0.674/x^+ - 3.44/\sqrt{x^+}}{Re\left[1 + 2.9\cdot 10^{-5}/(x^+)^2\right]} \tag{46}$$

$$x^+ = \frac{h}{d_h Re} \tag{47}$$

$$Re = \frac{\bar{v} d_h \bar{\rho}}{\bar{\mu}} \tag{48}$$

$$\bar{v} = \frac{\dot{m}}{A \cdot \bar{\rho}} \tag{49}$$

$$\dot{m} = \frac{1}{n} A_d \rho_1 v_1 = \frac{1}{n} A_d \rho_2 v_2 \tag{50}$$

The pressure losses in the entrance and exit PAR sections can be calculated in a similar way.

On the other hand, the force terms for the channel entrance and exit can be estimated as

$$F_{c1}=(p_1-\rho_1 g l_1-\Delta p_1)A_d-\left[p_1-\rho_1 g l_1-\Delta p_1+(1+\zeta_{c,1})\frac{\rho_1 \mathrm{v}_1^2}{2}-\rho_1\frac{\mathrm{v}_{c,1}^2}{2}\right]nA-A_d\rho_1\mathrm{v}_1^2+nA\rho_1\mathrm{v}_{c,1}^2 \quad (51)$$

$$F_{c2}=\left[p_2+\rho_2 g l_2+\Delta p_2+\frac{\rho_2\mathrm{v}_2^2}{2}-(1-\zeta_{c,2})\frac{\rho_2\mathrm{v}_{c,2}^2}{2}\right]nA-(p_2+\rho_2 g l_2+\Delta p_2)A_d+nA\rho_2\mathrm{v}_{c,2}^2-A_d\rho_2\mathrm{v}_2^2 \quad (52)$$

Equations (43-52) allow to find the limiting gas mass flow rate in an iterative procedure consisting of: an initial guess of the inlet gas velocity, determination of the gas density and viscosity profiles using the PAR model, estimation of pressure losses and the wall force, checking if the momentum balance (43) is fulfilled, and if this is not the case, finding a new better approximation of the inlet gas velocity.

3. RESULTS AND DISCUSSION

Predictions of the one-dimensional PAR model have been compared with experimental results (Drinovac, 2006; Reinecke et al., 2005) and with results of CFD modelling obtained for the test recombiner presented in Fig. 2. CFD calculations were performed with Ansys Fluent 14.5 and they were carried out for simplified two-dimensional PAR geometry. A 2-D computational grid consisted of 82,600 triangular and hexahedral elements in the central part of PAR, not counting mesh elements in the inlet and outlet PAR sections. Both convective and diffusive (including thermal diffusion) mass transport processes were accounted for in CFD simulations along with: convection of heat in gas, conduction of heat in gas and in the PAR body, and thermal radiation (Rożeń, 2013).

Side effects and heat exchange with the environment by the PAR housing are neglected in the mechanistic PAR model, hence the results of CFD calculations obtained for the central PAR channel were used for comparison purposes only. Prior to comparison, gas temperature and species concentration were mass averaged in subsequent lateral channel cross-sections.

All experimental data referenced in this work and model calculations were conducted for dry inlet gas (air-hydrogen mixture) of the initial temperature 298 K and atmospheric pressure 1.103×10^5 Pa. The inlet hydrogen concentration was changed from 0.5 to 5% v/v. The mechanistic model can also be used for high steam concentration in the inlet gas, observed during, e.g. coolant loss. This, however, requires kinetics of all adsorption, surface and desorption reactions to be modelled when calculating the local hydrogen recombination rate, as in CFD simulations conducted by e.g. Meynet et al. (2014).

Figures 3, 4 and 5 present profiles of catalyst temperature, gas temperature and hydrogen conversion degree as found along the central channel for different hydrogen concentrations (1, 2 and 4% v/v) and the gas velocity equal to 0.8 m/s at the inlet of the test recombiner; the actual entrance speed of gas to the central channel was higher due to flow contraction.

Two different kinetic models were used in calculations of the catalyst temperature: Kasemo's model – Eq. (2) and Schefer's model – Eq. (3). Figure 3 shows that in both cases a significant rise of the catalyst temperature was predicted with the increasing hydrogen concentration. Kasemo's kinetic model gives higher temperature in the lower part of the catalyst plate (small x) than Schefer's model. This relation is reversed in the upper part of the plate (high x), where differences between two kinetic models are small. It seems that catalytic hydrogen recombination proceeds mainly in the diffusion controlled regime except for a short entrance region where the concentration boundary layer is very thin. Hence, further calculations were conducted for Kasemo's kinetic model only.

Comparison with experimental data shows that the 1-D PAR model predicts the catalyst temperature well. In most cases, the difference between the measured and calculated temperature is comparable to the scatter of experimental results except for the lower section of the catalyst plate. The lack of

experimental data for the lower end of the catalyst plate ($x \approx 0$) does not allow to check if the catalyst temperature has or does not have a local maximum in this region as predicted by the PAR model. However, even if such a maximum exists, it could be probably less pronounced than that determined in model calculations.

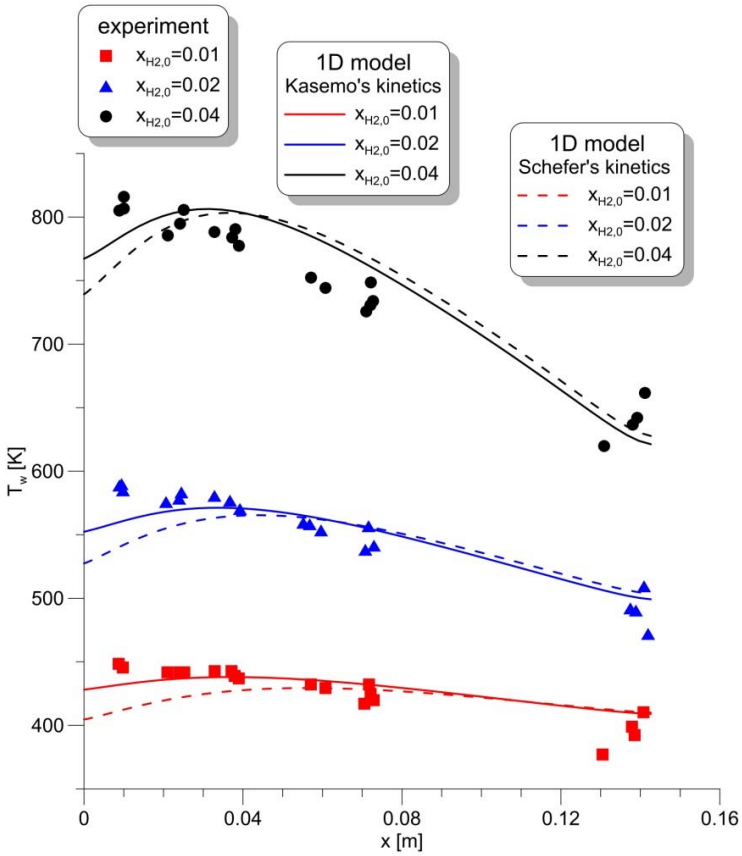

Fig. 3. Catalyst temperature profiles along the central PAR channel for v_1=0.8 m/s

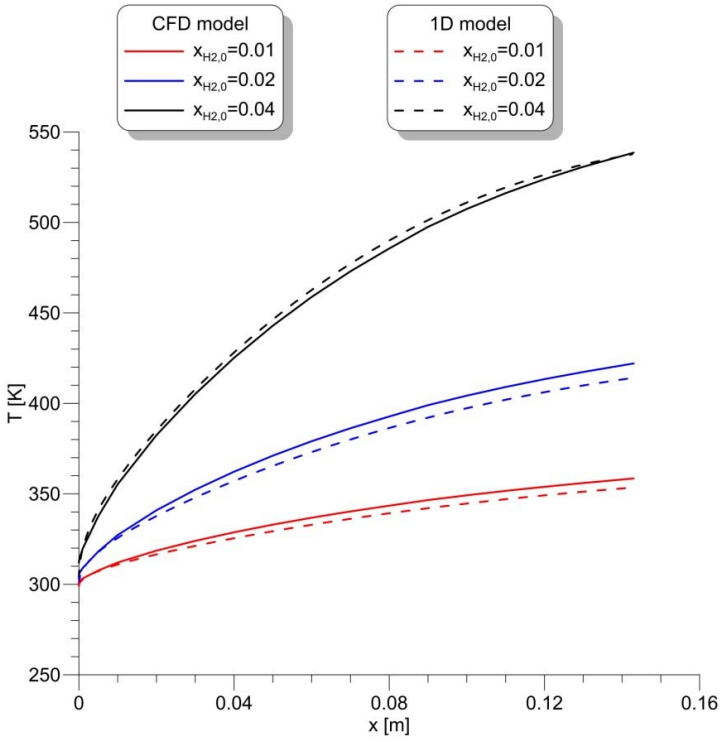

Fig. 4. Gas temperature profiles along the central channel for v_1=0.8 m/s

The observed differences between the model predictions and the experimental results may be caused by an overestimation of the total heat flux at the lower edges of the catalyst plates. Especially, the calculated radiative heat flux could be overestimated because of the model simplifications (black body surroundings) and too high values of the catalyst emissivity.

The gas mixture passing alongside the catalyst surface absorbs the reaction heat and its temperature increases up to a maximum at the channel outlet as indicated in Fig. 4.

Comparison of gas temperature profiles calculated with the 1-D PAR model with those obtained in CFD simulations shows relatively small differences. These deviations may be attributed to a dynamic formation of: gas velocity, gas temperature and concentration profiles in the channel entrance region accompanied by flow laminarisation (Rożeń, 2013), which could not be accounted for by a simple mechanistic model. Nevertheless, it seems that despite the application of the approximate calculation method of heat transfer coefficients for mixed convection – Eq. (12) – and neglecting heat transfer to the environment, the 1-D model gives accurate predictions of gas temperature.

Conversion degree of hydrogen calculated and plotted in Fig. 5 indicates that hydrogen recombination in the central channel of the test PAR is very effective. The fastest hydrogen depletion is observed in the channel entrance section. Then, hydrogen conversion gradually approaches its maximum values. The 1-D model predicts lower hydrogen conversion than the CFD model almost along the entire channel between the catalyst plates. This is probably caused by: very complex flow conditions, neglecting thermal diffusion in the model formulation and the approximate calculation method of mass transfer coefficients for assisted natural and forced convection.

It should be noted, however, that such high hydrogen conversion cannot be obtained in the side channels. In the case of the test PAR comprising just four catalyst plates, the inlet velocity 0.8 m/s, and the inlet hydrogen concentration 4% v/v, the overall hydrogen conversion is close to 70% as measured by Reinecke et al. (2005) and Drinovac (2006). It is always possible in this case to calibrate the model using measured experimentally hydrogen concentration in gas samples, taken along PAR, but then one has a semi-empirical formulation such as the REKO-DIREKT model by Reinecke et al. (2005).

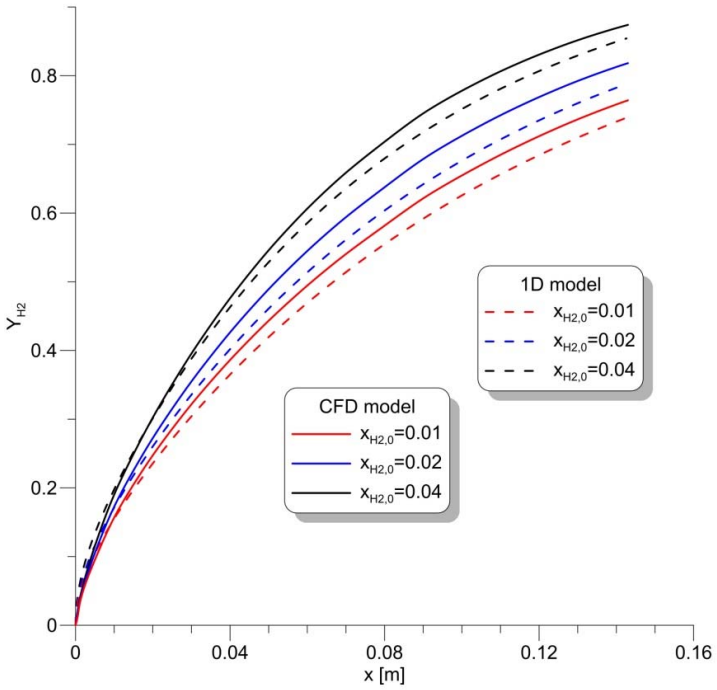

Fig. 5. Hydrogen conversion profiles along the central channel for v_1=0.8 m/s

So far, modelling has been conducted for known a priori inlet gas velocity. However, in real conditions the inlet gas velocity and consequently the cumulative rate of hydrogen recombination in PAR depend on the initial hydrogen concentration and the system geometry. Then, combining the PAR model with the macroscopic momentum balance – Eq. (43) – is the simplest way do determine actual operating conditions. Figure 6 presents a result of such approach in the case of the test recombiner, when the mechanistic and CFD models were used to determine the cumulative rate of hydrogen removal per unit volume of gas in the central channel $\Delta \dot{n}_{H_2}/V$ for different hydrogen inlet concentrations in the conditions of self-developed gas flow.

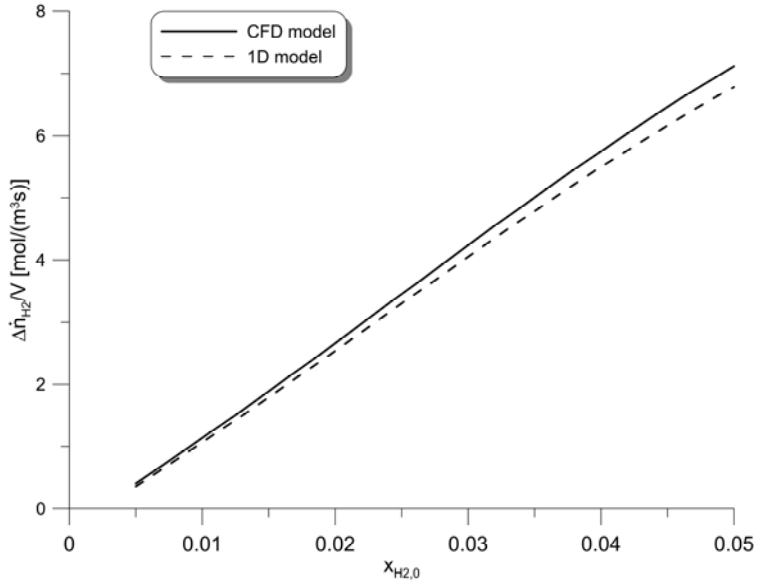

Fig. 6. Rate of hydrogen recombination per unit volume for self-developed gas flow

Analysis of Fig. 6 indicates that the 1-D model gives similar results to those obtained in CFD simulations. The observed differences range between 4 and 9% despite the fact that the mechanistic model has no adjustable parameters. In both cases growth of the hydrogen depletion rate vs. the inlet hydrogen concentration is practically linear. The average velocity of the cold hydrogen-rich gas at the PAR entrance (v_1), as determined in calculations, was ranging from 0.26 to 0.47 m/s respectively for the lowest ($x_{H2,0}$=0.005) and the highest ($x_{H2,0}$=0.05) initial hydrogen concentration.

A key question arising when designing a new recombiner is not only the selection of catalyst but also choosing the geometry of PAR, e.g. the number and dimensions of the catalyst plates, the distance between the plates (channel width) and the length of the PAR chimney. Usually engineers attempt to achieve the fastest hydrogen removal with the smallest and cheapest device, which can be easily installed in the containment of a nuclear reactor. The one-dimensional model of PAR combined with the chimney draft equation can be used to conduct initial calculations, for example to find out the optimal distance between the catalyst plates. Results of such preliminary calculations performed for the recombiner with the same length of: the inlet section (l_1), the catalyst plates (h) and the chimney (l_2) as the test recombiner (Fig. 2) are presented in Fig. 7.

According to Fig. 7, the cumulative hydrogen recombination rate per unit volume of the single channel displays a maximum for channel width close to 10÷10.5 mm. On the other hand, the optimum distance required for the fastest natural heat convection per unit volume from the channel walls, calculated from Eqs (13-18), lies in the range from 6 to 7 mm depending on the temperature of the wall surface. Hence, when looking for an optimum channel width, one should model all key processes occurring in PAR instead of considering the reaction heat removal only. Figure 7 also shows that the initial hydrogen concentration has a very small effect on the optimal distance between the catalyst plates. This allows to limit the optimisation procedure to the nominal hydrogen concentration.

PAR efficiency can be further improved by optimising the chimney length and dimensions of the catalyst plates but then the cumulative recombination rate should be denominated by the entire volume of the PAR box.

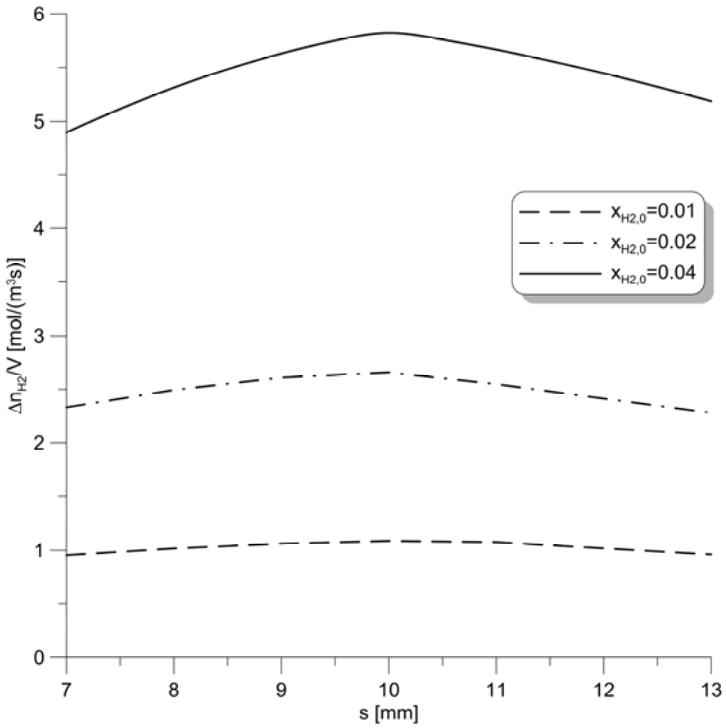

Fig. 7. Effect of channel width on the rate of hydrogen recombination per unit volume for self-developed gas flow

4. CONCLUSIONS

The one-dimensional mechanistic model of the catalytic hydrogen recombiner presented in this work can well predict the profiles of: catalyst temperature, gas temperature and gas composition along the single recombiner channel. The model requires neither fitting to reference experimental data nor initial calibration. It has been validated by the results of experiments available in the literature and the results of CFD simulations. The model is relatively simple, uses correlations for heat and mass transfer coefficients generally accessible in engineering handbooks and does not require sophisticated numerical methods or large CPU overhead. Therefore, the model can be used for quick engineering calculations, preliminary optimisation of PAR geometry, testing different kinetic models of the catalytic hydrogen recombination or it can be assembled as subroutine with commercial CFD codes. In future, the model can be improved by including: mass and heat accumulation effects, longitudinal mass dispersion, more realistic calculation of the radiative heat flux and full, instead of simplified, kinetics of hydrogen recombination.

This work was financially supported by The National Centre for Research and Development in Poland (grant no. SP/J/7/170071/12).

SYMBOLS

A	channel cross-section area, m^2
A_d	PAR cross-section area, m^2
A_w	side surface area of the catalyst plate, m^2

A_1, A_2	PAR inlet and outlet surface area, m^2
b	PAR width, m
c_i	molar concentration of i–th reactant, mol/m^3
c_p	heat capacity of gas, J/(kg·K)
$c_{p,s}$	heat capacity of stainless steel, J/(kg·K)
D_i	molecular diffusivity of i-th reactant, m^2/s
d_h	hydraulic diameter of the channel, m
F	wall force, N
$F_{c,1}$, $F_{c,2}$	wall force corrections, N
F_{i-j}	configuration coefficient of radiant surfaces
f	friction coefficient
g	gravitational acceleration, m/s^2
H	gas enthalpy, J/kg (J/mol)
h	height of the catalyst plates, m
k	mass transfer coefficient, $kg/(m^2 \cdot s)$
l_1, l_2	length of the inlet and outlet PAR sections, m
M_i	molar mass of i-th reactant, kg/mol
m_g	mass of gas in PAR, kg/mol
$\dot{m}$	mass flow rate of gas in the central channel, kg/s
Nu	Nusselt number
n	number of channels
Pe	thermal Peclet number
Pe_i	concentration Peclet number
Pr	Prandtl number
p	gas pressure, Pa
q	total heat flux, W/m^2
q_r	radiative flux at the catalyst surface, W/m^2
R	universal gas constant, (=8.3143 J/(mol·K))
Ra	Rayleigh number
Re	Reynolds number
$\tilde{r}_{H_2}$	local rate of the recombination reaction, $mol/(m^2 \cdot s)$
Sc_i	Schmidt number of i-th reactant
Sh_i	Sherwood number of i-th reactant
s	distance between the catalyst plates (channel width), m
T	gas temperature, K
T_e	surroundings temperature, K
T_f	film temperature, K
T_m	mean temperature, K
T_w	catalyst plate temperature, K
V	volume of the central channel, m^3
v	gas velocity in inlet (outlet) PAR sections, m/s
v_c	gas velocity in the channel, m^3
w_i	mass fraction of i-th reactant in gas stream
$w_{w,i}$	mass fraction of i-th reactant in gas at the catalyst surface
x	coordinate along the catalyst plate ($0 \le x \le h$), m
x_i	mole fraction of i-th reactant in gas stream
x^+, x^*	dimensionless coordinates
Y_{H2}	conversion degree of hydrogen

Greek symbols

α	heat transfer coefficient, $W/(m^2 \cdot K)$

β_i	concentration coefficient of volume expansion
β_T	thermal coefficient of volume expansion, 1/K
$\Delta\dot{n}_{H_2}$	cumulative hydrogen recombination rate, mol/s
Δp	pressure loss in the central channel, Pa
Δp_1, Δp_2	pressure losses in PAR inlet and outlet sections, Pa
δ	width of the catalyst plate, m
ε_c	catalyst surface emissivity
ε_s	stainless steel emissivity
λ	thermal conductivity of gas, W/(m·K)
λ_s	thermal conductivity of stainless steel, W/(m·K)
μ	dynamic viscosity of gas, m^2/s
ν	kinematic viscosity of gas, m^2/s
ν_i	stoichiometric coefficient of *i*-th reactant
ρ	gas density, kg/m^3
ρ_s	stainless steel density, kg/m^3
σ	Stefan-Boltzmann constant (=$5.6705 \cdot 10^{-8}$ $W/(m^2 \cdot K^4)$)
ζ	minor loss coefficient for PAR entrance (exit)
ζ_c	minor loss coefficient for an entrance (exit) to a channel between catalyst plates

Overlines

–	mean along distance *x*
~	per mole

Subscripts

f	forced convection
i	i-th reactant
n	natural convection
1	entrance, lower edge
2	exit, upper edge

REFERENCES

Areva Inc., 2014. AREVA Passive autocatalytic recombiner, Retrieved in September 2014, from http://us.areva.com/home/liblocal/docs/Solutions/literature/G-008-V1PB-2011-ENG_ PAR_reader.pdf.

Avakian G., Braillard O., 1999. Theoretical model of hydrogen recombiner for a nuclear power plant. *7th International Conference on Nuclear Engineering*. Tokyo, Japan, April 19-23, 1999.

Bird R.B., Stewart W.E., Lightfoot E.N., 2002. *Transport phenomena*. 2nd edition, John Wiley & Sons, New York.

Churchill S.W., 1977. A comprehensive correlating equation for laminar, assisting, forced and free convection. *AIChE J.*, 23, 10-16. DOI: 10.1002/aic.690230103.

Crane Co., 2009. *Flow of fluids through valves, fittings and pipe*. Technical Paper No. 410, Crane Company, Stamford, U.S.A.

Drinovac P., 2006. *Experimental studies on catalytic hydrogen recombiners for light water reactors*. PhD Thesis. RWTH Aachen University.

Euro Inox, 2014. *Tables of Technical Properties of Stainless Steels*. The European Stainless Steel Development Association. Retrieved in August 2014, from http://www.euro-inox.org/technical_tables.

Fridell E., Rosen A., Kasemo B., 1994. A laser-induced fluorescence study of OH desorption from Pt in H_2O/O_2 and H_2O/H_2 mixtures. *Langmuir*, 10, 699-708. DOI: 10.1021/la00015a018.

Gera B., Sharma P.K., Singh R.K., 2012. 2D numerical simulation of passive autocatalytic recombiner for hydrogen mitigation. *Heat Mass Transf.*, 48, 591-598. DOI 10.1007/s00231-011-0906-5.

Heitsch M., 2000. Fluid dynamic analysis of a catalytic recombiner to remove hydrogen. *Nucl. Eng. Des.*, 201, 1–10. DOI: 10.1016/S0029-5493(00)00259-4.

IAEA-TECDOC-1196, 2001. *Mitigation of hydrogen hazards in water cooled powered reactors*. IAEA, Vienna.

IAEA-TECDOC-1661, 2011. *Mitigation of hydrogen hazards in severe accidents in nuclear power plants*. IAEA, Vienna.

Jimenez M.A., Martin-Valdepanas J.M., Martin-Fuentes F., Fernandez J.A., 2007. A detailed chemistry model for transient hydrogen and carbon monoxide catalytic recombination on parallel flat Pt surfaces implemented in an integral code. *Nucl. Eng. Des.*, 237, 460-472. DOI:10.1016/j.nucengdes.2006.09.002.

Meynet N., Bentaib A., Giovangigli V., 2014. Impact of oxygen starvation on operation and potential gas-phase ignition of passive auto-catalytic recombiners. *Combust. Flame, 161*, DOI: 2192-2202. 10.1016/j.combustflame.2014.02.001.

NEA/CSNI R(2014)8, 2014. *Status report on hydrogen management and related computer codes*. OECD, 117-166.

Poling B.E., Prausnitz J.M., O'Connell J.P., 2001. *The properties of gases and liquids*. 5th edition, McGraw-Hill Companies Inc., Boston.

Prabhudharwadkar D.M., Aghalayam P.A., Iyer K.N., 2011. Simulations of hydrogen mitigation in catalytic recombiner. Part-I: Surface chemistry modelling. *Nucl. Eng. Des.*, 241, 1746-1757. DOI: 10.1016/j.nucengdes.2010.09.032.

Prabhudharwadkar D.M., Aghalayam P.A., Iyer K.N., 2011. Simulations of hydrogen mitigation in catalytic recombiner. Part-II: Formulation of the CFD model. *Nucl. Eng. Des.,* 241, 1758-1767. DOI: 10.1016/j.nucengdes.2011.01.013.

Press W.H., Teukolski S.A., Vetterling W.T., Flannery B.P., 1992. *Numerical recipes in C. The art of scientific computing*. 2nd edition, Cambridge University Press, Cambridge.

Reinecke E.A., Boehm J., Drinovac P., Struth S., Tragsdorf I.M., 2005. Modelling of catalytic recombiners: Comparison of REKO-DIREKT calculations with REKO-3 experiments. *International Conference Nuclear Energy for New Europe*. Bled, Slovenia, September 5-8, 2005.

Reinecke E.A., Bentaib A., Kelm S., Jahn W., Meynet N., Caroli C., 2010. Open issues in the applicability of recombiner experiments and modelling to reactor simulations. *Prog. Nucl. Energ.*, 52, 136-147. DOI:10.1016/j.pnucene.2009.09.010.

Rinnemo M., Deutschmann O., Behrendt F., Kasemo B., 1997. Experimental and numerical investigation of the catalytic ignition of mixtures of hydrogen and oxygen on platinum. *Combust. Flame*, 111, 312-326. DOI: 10.1016/S0010-2180(97)00002-3.

Rohsenow W.M., Hartnett J.P., Cho Y.I., 1998. *Handbook of heat transfer*. 3rd edition, McGraw-Hill Companies Inc., New York.

Rożeń A., 2013. Modelling of a passive catalytic recombiner for hydrogen mitigation by CFD methods. *International Conference Nuclear Energy for New Europe*. Slovenia, Bled, September 9-12, 2013.

Schefer R.W., 1982. Catalyzed combustion of H_2/air mixtures in a flat plate boundary layer: II. Numerical model. *Combust. Flame*, 45, 171-190. DOI: 10.1016/0010-2180(82)90043-8.

Shah, R.K., 1978. A correlation for laminar hydrodynamic entry length solutions for circular and non-circular ducts. *ASME J. Fluids Eng.*, 100, 177–179. DOI:10.1115/1.3448626.

Taunton J.W., Lightfoot E.N., Stewart W.E., 1970. Simultaneous free-convection heat and mass transfer in laminar boundary layers. *Chem. Eng. Sci.*, 25, 1927-1937. DOI: 10.1016/0009-2509(70)87010-5.

Received 23 September 2014
Received in revised form 12 December 2014
Accepted 18 December 2014